ResearchGate

See discussions, stats, and author profiles for this publication at: https://www.researchgate.net/publication/330846768

Structural and electrical properties of transparent conductor SrVO3 thin films grown using radio frequency sputtering deposition

Article *in* Journal of Vacuum Science & Technology A Vacuum Surfaces and Films · March 2019

DOI: 10.1116/1.5054666

CITATIONS
10

READS
504

3 authors:

Dae Ho Jung
Kyung Hee University
20 PUBLICATIONS **137** CITATIONS

SEE PROFILE

Hyeon Seob So
Kyung Hee University
18 PUBLICATIONS **354** CITATIONS

SEE PROFILE

Hosun Lee
Kyung Hee University
129 PUBLICATIONS **1,995** CITATIONS

SEE PROFILE

Some of the authors of this publication are also working on these related projects:

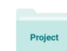

Transparent oxide films: conductors and semiconductors View project

All content following this page was uploaded by Hosun Lee on 27 February 2019.

The user has requested enhancement of the downloaded file.

Structural and electrical properties of transparent conductor $SrVO_3$ thin films grown using radio frequency sputtering deposition

Dae Ho Jung, Hyeon Seob So, and Hosun Lee

Citation: Journal of Vacuum Science & Technology A **37**, 021507 (2019); doi: 10.1116/1.5054666
View online: https://doi.org/10.1116/1.5054666
View Table of Contents: https://avs.scitation.org/toc/jva/37/2
Published by the American Vacuum Society

CrossMark

Structural and electrical properties of transparent conductor $SrVO_3$ thin films grown using radio frequency sputtering deposition

Dae Ho Jung, Hyeon Seob So, and Hosun Lee[a)]
Department of Applied Physics, Institute of Natural Sciences, Kyung Hee University, Yong-In 17104, Republic of Korea

(Received 1 September 2018; accepted 4 January 2019; published 22 January 2019)

Transparent conductor $SrVO_3$ thin films were grown on $(LaAlO_3)_{0.3}(Sr_2AlTaO_6)_{0.7}$ (LSAT), SiO_2/Si, $LaAlO_3$, and sapphire substrates using RF magnetron sputtering deposition with commercial $SrVO_3$ targets at temperatures as low as 400 °C. Considering the complex phases of $SrVO_3$ material systems, the growth temperature and sputtering gases were optimized and precisely controlled to yield a transparent and conductive $SrVO_3$ phase. The authors used a mixed gas atmosphere of Ar and H_2 during growth for reduction. Structural and morphological properties of all $SrVO_3$ films were investigated using x-ray diffraction (XRD), high-resolution transmission electron microscopy (HRTEM), and scanning electron microscopy. XRD and HRTEM showed a highly crystalline cubic phase of $SrVO_3$ films. In addition, HRTEM showed that a superstructure along the [100] direction could be formed due to Jahn-Teller distortion in the cubic phase of $SrVO_3$ films. The authors obtained a resistivity of $0.2 \times 10^{-3}\,\Omega\,cm$, mobility of $1.82\,cm^2/(V\,s)$, and carrier concentration of $1.57 \times 10^{22}\,cm^{-3}$ for $SrVO_3$/LSAT films. Optical transmittance was measured as 88% at a photon wavelength of 633 nm for 39-nm-thick $SrVO_3$ films. Using x-ray photoemission spectroscopy (XPS) and its depth profile analysis, the authors investigated chemical compositions and binding energies of Sr, V, and O atoms in $SrVO_3$ films, and their depth profiles. The authors found a correlation between the resistivities and XPS binding energy spectra for $SrVO_3$ films as functions of film thickness and substrates. *Published by the AVS.* https://doi.org/10.1116/1.5054666

I. INTRODUCTION

Highly conductive and yet highly transparent materials can be used for applications such as electric devices, displays, and energy devices. However, the two characteristics of transparency and conductivity are mutually exclusive and it is difficult to find transparent conductors that use electrons and holes as charge carriers.[1] In general, the resistivity of thin films is higher than that of bulk materials due to the surface scattering of electron carriers. Transparent electrodes are used for optoelectronics devices. Presently, ITO films are the most widely used transparent electrodes. Furthermore, SnO_2:X (X: F, Sb) and ZnO:X (X: Al, Ga) are also used for transparent conducting oxide (TCO) materials.[2] These TCO materials have a band gap energy larger than 3 eV and are transparent in the visible spectral range, and their resistivities are less than $10^{-3}\,\Omega\,cm$.

To increase the performance of the TCO, it is necessary to increase the carrier concentrations, while maintaining a high mobility. ITO films have high transparency and high conductivity. However, the element indium (In) is becoming scarcer and its resistivity is high in ultrathin films due to increased surface scattering. Therefore, we need new TCO materials. SnO_2 films are cheap and chemically stable whereas their resistivities are high and processing temperature is relatively high. ZnO films have excellent electrical and optical properties, comparable to those of ITOs, whereas they are chemically unstable and are vulnerable to acid and alkalinity. Recently, transition metal oxides (TMO) were proposed as promising TCO materials.[3,4] Zhang *et al.* proposed TMO as transparent conductors such as $SrVO_3$ and $CaVO_3$ films.[4] These perovskite oxide materials have strongly correlated electrons. Their carrier electron masses increase due to renormalization, and $SrVO_3$ and $CaVO_3$ films become transparent in the visible spectral range with low screened plasma energy (<1.33 eV).

Metallic $SrVO_3$ crystals have a cubic perovskite structure, and the lattice parameter is a = 3.842 Å. Valance bands of $SrVO_3$ crystals originate from oxygen 2p orbitals. Vanadium 3d orbitals are split into e_g group (duplet state) and t_{2g} group (triplet state) due to the crystal field effect.[4] Here, the t_{2g} group forms the conduction band. The interband transition is weak in the visible spectral range. $SrVO_3$ forms a simple Fermi liquid system. The electrons are strongly correlated and spectral weight transfer occurs. The imaginary dielectric function of $SrVO_3$ films is still as large as 1 in the 1.2–2.7 eV spectral range, and ultrathin films less than 30 nm are required for greater than 90% transmittance in the visible range. Since the mean free path of electron carriers in the $SrVO_3$ films is 5.6 nm,[4] low resistivity persists in ultrathin (≈10 nm) $SrVO_3$ film.

Growth of cubic phase $SrVO_3$ films was carried out using various growing methods, including hydride MBE,[4,5] pulsed laser deposition (PLD),[6,7] electron-beam evaporation,[8,9] and chemical vapor deposition.[10] There are few reports on sputtering deposition of cubic phase $SrVO_3$ films.[11] We note that Sharma *et al.* grew orthorhombic $SrVO_3$ films, which were both transparent and highly resistive, using sputtering deposition.[12]

Several substrates have been used to grow $SrVO_3$ films: $(LaAlO_3)_{0.3}(Sr_2AlTaO_6)_{0.7}$ (LSAT),[4–6] $LaAlO_3$ (LAO),[13] $SrTiO_3$,[7,14,15] Si,[16] and yttria-stablized zirconia (YSZ)/Si.[13]

[a)]Electronic mail: hlee@khu.ac.kr

LSAT substrates have similar lattice constants to $SrVO_3$ films, and $SrVO_3$ films grown on LSAT substrates showed the best electrical and optical properties compared to other substrates.[4,5] Commercial $SrVO_3$ targets are composed of a $Sr_2V_2O_7$ phase, and a high growth temperature under vacuum deposition or H_2 gas is needed for a reducing environment to grow cubic phase $SrVO_3$ films.[5,10] Hybrid MBE methods require high temperature growth, as high as 900 °C, as well as appropriate stoichiometry of the $SrVO_3$ film for high conductivity.[17] However, Jung *et al.*[11] reported that Sr deficiency ($Sr_{0.9}VO_3$) was required and low temperature growth as low as 10 °C can be used for the growth of high conductivity $SrVO_3$ films.

Sputtering growth of $SrVO_3$ films has not been reported so far in the literature. Furthermore, using commercial $SrVO_3$ targets (actually $Sr_2V_2O_7$ targets) is very desirable for the sputtering growth of $SrVO_3$ films because of low cost and simple growth methods, which is essential for industrial applications.

In this work, we used a RF magnetron sputtering deposition method to grow transparent conductor $SrVO_3$ films on various substrates in a mixture of Ar and H_2 gas using a commercial $Sr_2V_2O_7$ target. We investigated the structural, optical, and electrical properties of $SrVO_3$ films. We found a correlation among resistivity, V^{4+}/V^{5+} ratio, and the composition gradients in Sr, V, and O atoms as a function of $SrVO_3$ film thicknesses. We found that almost lattice-matched LSAT substrates provided the lowest resistivity values and high optical transmittance for $SrVO_3$ films at a growth temperature as low as 400 °C. We found a superstructure along the [100] direction, which could be formed due to Jahn-Teller distortion in the cubic phase of $SrVO_3$ films.

II. EXPERIMENT

$SrVO_3$ thin films with thicknesses between 39 and 90 nm were grown on a-plane, c-plane, r-plane, and m-plane sapphire, Si, SiO_2/Si, LAO, and LSAT substrates under identical conditions by sputtering deposition using commercial $SrVO_3$ targets (99.5 wt. %). Nominal $SrVO_3$ targets from RNDKOREA (Republic of Korea) and LTS Research Laboratories, Inc. (USA) were used. The targets were actually composed of a $Sr_2V_2O_7$ phase. Considering the complex phases of the $SrVO_3$ material system, the growth temperature and sputtering gas atmosphere were optimized and precisely controlled to yield conductive $SrVO_3$ films of cubic phase. Sputtering pressure was set at 6 mTorr with 25% $H_2/(Ar + H_2)$ gas. The flow rate was 10–20 sccm. $SrVO_3$ films were grown at 350–500 °C. After sputtering, $SrVO_3$ films were annealed. We note that only $Sr_2V_2O_7$ phase was grown using Ar or a mixture of Ar and O_2 gas.

The structural and morphological properties of all $SrVO_3$ films were studied using Θ-2Θ x-ray diffraction (XRD) spectroscopy, grazing incidence of angle x-ray diffraction (GIXRD), high-resolution field-effect scanning electron microscopy (FE-SEM), and high-resolution transmission electron microscopy (HRTEM). Θ-2Θ XRD was performed for $SrVO_3$ films using standard XRD equipment. GIXRD was measured to enhance XRD signals from $SrVO_3$ films with Cu Kα x-ray line (wavelength 1.5406 Å) using an x-ray diffractometer (Model: SmartLab, Rigaku). Resistivities were measured using a Keithley 4200-SCS system. Hall mobilities (μ_{Hall}) and carrier concentrations (N_{Hall}) were determined via Hall effect measurements (Model: H-50, MMR) in the Van der Pauw configuration. The electronic structure, atomic compositions, and depth profiles of $SrVO_3$ films were investigated using x-ray photoemission spectroscopy (XPS) (Model: K-Alpha, Thermo Electron). The incident x-ray photon source was Al Kα line (1486.6 eV). Surface morphologies of the $SrVO_3$ thin films were investigated via FE-SEM (Model: Merlin, Carl Zeiss). Cross-sectional HRTEM data were also measured (Model: JEM-2100F, JEOL). Raman scattering spectra were measured by using a McPherson 207 spectrometer equipped with a nitrogen-cooled charge-coupled-device array detector. $SrVO_3$ films were excited by a 488 nm diode laser with a power less than 0.5 mW to minimize heating effects.

III. RESULTS AND DISCUSSION

Figure 1 shows the FE-SEM images of $SrVO_3$ films grown on (a) (100) LSAT, (b) (100) $LaAlO_3$, and (c) SiO_2/Si substrates. In Fig. 1(a), $SrVO_3$ films grown on LSAT substrates showed grains with sizes of 88 × 88 nm. In Figs. 1(b) and 1(c), $SrVO_3$ films grown on $LaAlO_3$ and SiO_2/Si substrates showed grains with size of 74 × 74 nm and 85 × 85 nm, respectively.

Figures 2(a)–2(f) show the GIXRD pattern of $SrVO_3$ films grown on LSAT substrates with the film thickness: (a) 39 nm, (b) 51 nm, (c) 64 nm, (d) 77 nm, (e) 90 nm, and (f) SiO_2/Si substrates, and Figs. 2(g) and 2(h) show the (210) lattice parameter and the size of nanocrystallites, respectively.

We found a (210) GIXRD peak at 2θ ($d_{(210)}$) = 52.44° (1.744 Å), 52.52° (1.742 Å), 53.07° (1.724 Å), 53.67° (1.706 Å), and 53.50° (1.713 Å) for the film thickness of 39, 64, 51, 77, and 90 nm, respectively, as shown in Fig. 2(g).[18] The average error bar was ±0.002 Å. The same peak was measured at 53.17° (1.722 Å) for $SrVO_3/SiO_2$/Si. $SrVO_3$/LSAT films showed a single phase for all the films except the 51 nm-thick films in Fig. 2(b). The $SrVO_3$ film of 51 nm thickness in Fig. 2(b) showed 28.88° and 55.01° peaks in addition to the (210) 52.52° peak. The 28.88° peak arose from either a tetragonal $Sr_2V_2O_7$ (204) phase or orthorhombic $SrVO_3$ (020) phase. The 55.01° peak arose from the orthorhombic $SrVO_3$ (311) peak. The decrease of (210) lattice parameters with increasing film thickness may be due to the decrease of oxygen deficiency or other defects. Or it could be due to strain relaxation with increasing film thickness. Using XRD, Rey *et al.* measured the (210) lattice parameters as 1.723 and 1.717 Å for $SrVO_{2.88}$ and $SrVO_3$, respectively.[19] Brahlek *et al.* also reported that the lattice constants were minimized when defect densities were lowest and $SrVO_3$ was stoichiometric.[17] In this sense, the 77-nm-thick $SrVO_3$ film has the fewest defect densities, i.e., the highest stoichiometry [Fig. 2(g)]. The lattice parameters for bulk $SrVO_3$ crystals are a = 3.842 Å for cubic phase,[4] and a = 6.156 Å, b = 7.701 Å, c = 5.367 Å for orthorhombic phase.[12]

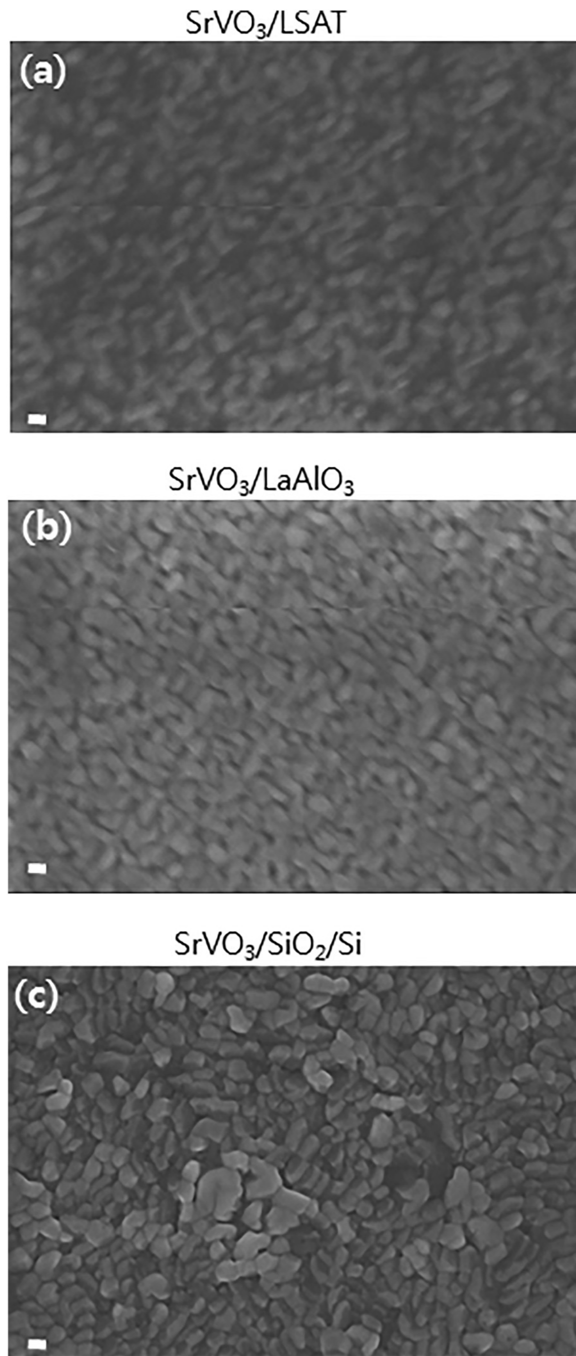

FIG. 1. FE-SEM images of $SrVO_3$ films (thickness: 77 nm) grown on (a) LSAT, (b) $LaAlO_3$, and (c) SiO_2/Si substrates. The marker size denotes 100 nm.

Figure 2(h) shows the size of the nanocrystallites estimated from the FWHM of the (210) XRD peak. The Scherrer equation was employed as follows:

$$d = \frac{K\lambda}{\beta\cos\theta}, \tag{1}$$

where K is the shape factor (= 0.9), λ is the x-ray wavelength of the Cu Kα line, β is the FWHM in radians, θ is the Bragg angle, and d is the mean nanocrystallite size. The nanocrystallite size was about 8 nm up to 51 nm film thickness, and then decreased abruptly to approximately 4.5 nm as the film thickness increased further, as shown in Fig. 2(h). The average error bar was ±0.3 nm. Since the grain sizes shown in Fig. 1 were an order of magnitude larger than the nanocrystallite size measured with XRD, the grains must be composed of smaller nanocrystallites.

We found a mixture of cubic and orthorhombic phases from $SrVO_3$ films grown on SiO_2/Si, namely, 28.97° (020), 43.59° (212), 49.27° (123) for orthorhombic $SrVO_3$ phases; 53.17° (210) for cubic $SrVO_3$ phases; and 55.29°(330) for the orthorhombic $Sr_2V_2O_7$ peak.[20,21] Some of the orthorhombic $Sr_2V_2O_7$ peaks may be identified as a tetragonal phase of $Sr_2V_2O_7$ such as 28.97° (204), 43.59° (2 0 10), and 49.27° (1 1 13). Since orthorhombic phases of $SrVO_3$ films are insulating, we expect that $SrVO_3$ films grown on SiO_2/Si will have higher resistance than $SrVO_3$ films grown on LSAT. XRD showed that LSAT substrates had a dominant (400) phase with minor phases of (222), (442), and (420) (not shown here).

Figure 3 shows the HRTEM image of $SrVO_3$ films grown on LSAT with 90 nm film thickness: (a) cross-sectional HRTEM data and fast Fourier transform (FFT) transform from (b) Region 1 and (c) Region 2 in (a). Figure 3 shows highly crystalline $SrVO_3$ films grown on LSAT with (b) FFT pattern of cubic phase of ABO_3 cubic structure and (c) FFT pattern of super-structured cubic phases. We note that the satellite peaks in Fig. 3(c) arose from the formation of a super structure along the [200] direction of $SrVO_3$ phase. Using GATAN analysis software, we determined the direction of FFT spots, as in Fig. 3(b). We found lattice parameters of 2.771 Å (Region 1) and 2.755 Å (Region 2) for a (110) cubic $SrVO_3$ phase. We observed lattice parameters (100) 3.969 Å and (110) 2.773 Å from LSAT substrates using HRTEM (not shown here).[22] According to FFT images of both $SrVO_3$ films and LSAT substrates, the $SrVO_3$ film orientation was [100] direction, considering the orientation of the LSAT substrate. We note that the lattice parameter 3.969 Å (100) of the LSAT substrate is larger than the reference value of 3.870 Å.[23] However, the XRD data of the LSAT substrate in this work provided the lattice parameter of (100) LSAT substrate as 3.858 Å, which is similar to the reference value. HRTEM is a local probe whereas XRD is a nonlocal probe. The large lattice parameter of 3.969 Å (100) of the LSAT substrate which was measured using HRTEM should be a local phenomenon and could be due to either local interface strain or local expansion of lattice constant due to oxygen vacancy.

Figure 4 shows (a) the binding energy spectra of vanadium ions for $SrVO_3$ films with various thicknesses measured using XPS, and the depth profiles of $SrVO_3$ films (thickness: 77 nm) grown on (b) LSAT, (c) SiO_2/Si, and (d) LAO. We found that the V^{5+} valence state transformed to V^{4+} as the $SrVO_3$ film thicknesses increased. The valence state of the V atom in stoichiometric $SrVO_3$ films should be V^{4+}. The V^{5+} valence state is attributed to the $Sr_2V_2O_7$ phase. It appears that the surface layers of $SrVO_3$ films were oxidized to the $Sr_2V_2O_7$ phase. The binding energy of V decreased from 516.83 eV (39 nm, V^{5+}) to 516.30 eV (77 nm, V^{4+}) as the film thickness increased.[24,25] The XPS depth profiles in Fig. 4(b) show that $SrVO_3$ films grown on LSAT substrates

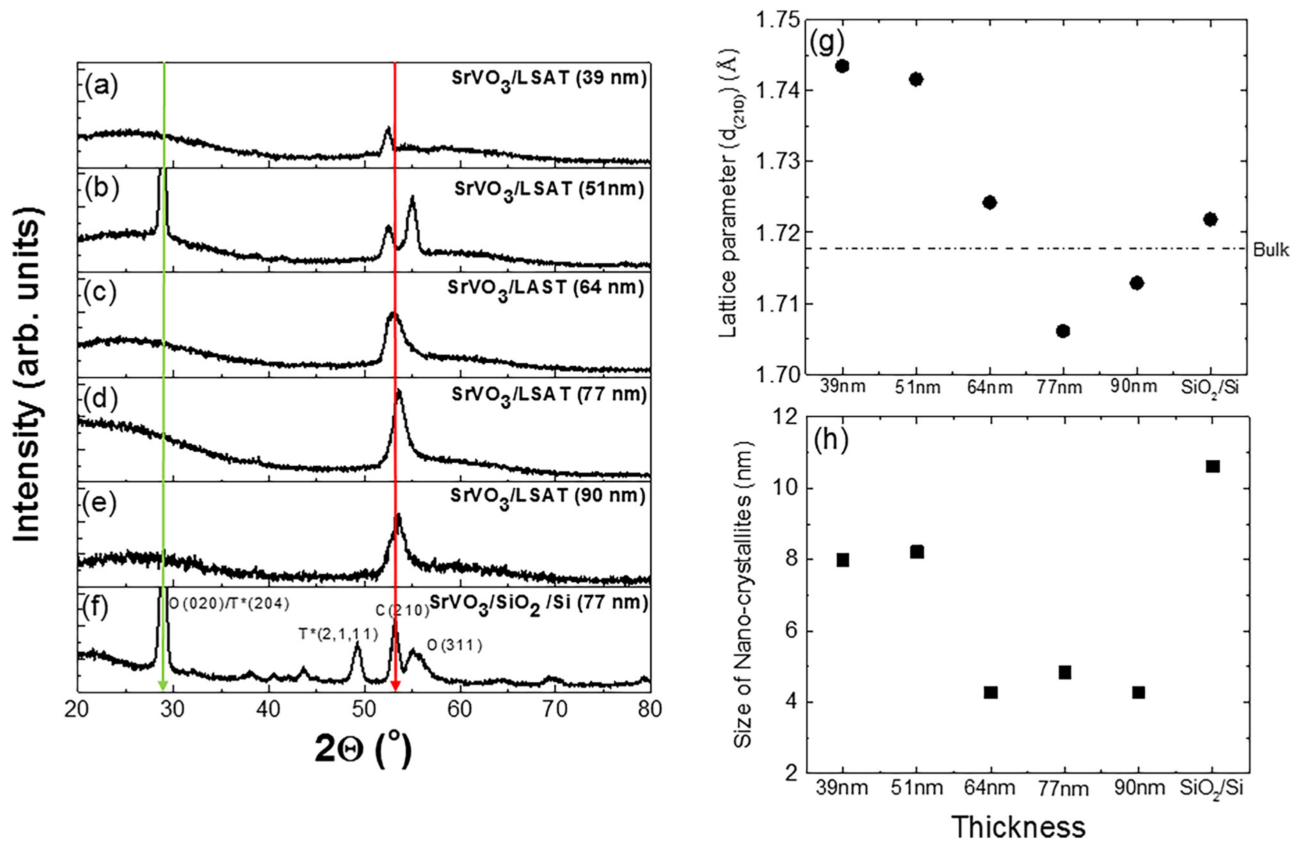

FIG. 2. GIXRD pattern of $SrVO_3$ films grown on LSAT films of thickness: (a) 39 nm, (b) 51 nm, (c) 64 nm, (d) 77 nm, (e) 90 nm, and (f) SiO_2/Si substrates. (g) and (h) show the (210) lattice parameter and nanocrystallite size, respectively, as a function of $SrVO_3$ films thickness. The error bars were ±0.002 Å and ±0.3 nm, respectively. In (f), C and O denote cubic and orthorhombic phases, respectively, of the $SrVO_3$ film, and T* denotes tetragonal phase of the $Sr_2V_2O_7$ film. In (g), dashed line denotes bulk value.

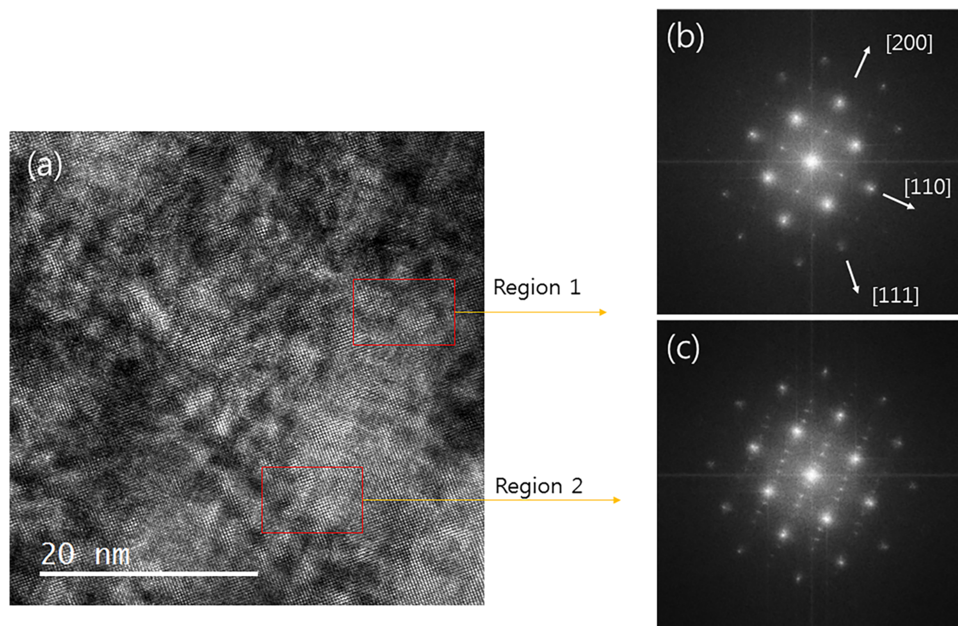

FIG. 3. HRTEM images of $SrVO_3$ films grown on LSAT with 90 nm thickness: (a) cross-sectional HRTEM data and FFT transform from (b) Region 1 and (c) Region 2 in (a).

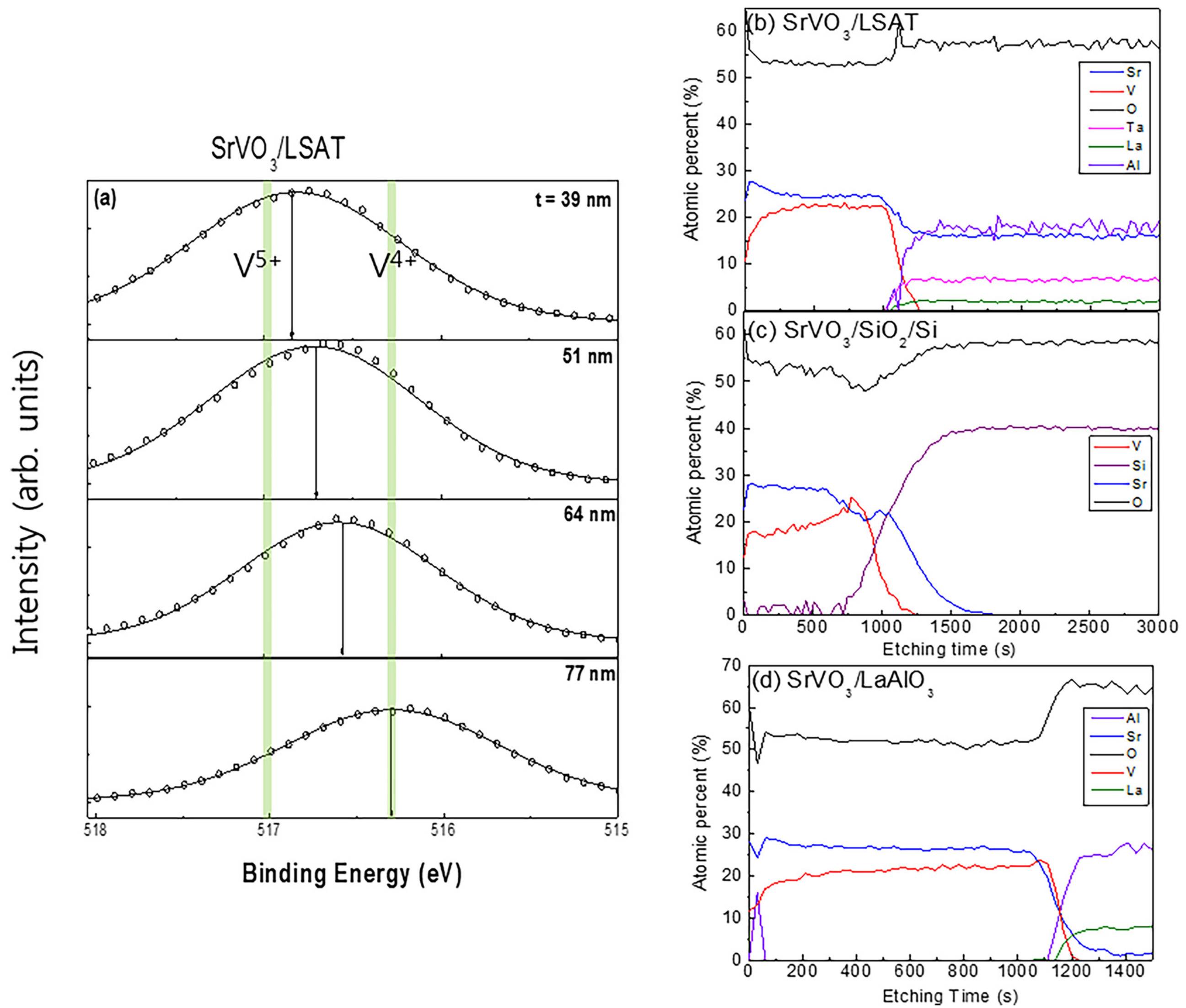

FIG. 4. (a) Binding energy spectra of vanadium ions for $SrVO_3$/LSAT films with various thicknesses measured using XPS, and the depth profiles of $SrVO_3$ films (thickness: 77 nm) grown on (b) LSAT, (c) SiO_2/Si, and (d) $LaAlO_3$ substrates.

showed homogeneous distribution of $SrVO_3$ compositions and sharp interfaces between $SrVO_3$ films and LSAT substrates. However, we found an oxidized surface layer of about 10 nm. Furthermore, the surface composition of $SrVO_3$ films was V deficient with excess Sr. In Fig. 4(c), $SrVO_3$ films grown on SiO_2/Si substrates showed excess Sr and V deficiencies compared to $SrVO_3$ films grown on LSAT, as in Fig. 4(b), and showed a Sr_xSi_yO phase near interfaces. The $Sr_xSi_yO_z$ phase near the interface is consistent with the literature.[11,15,26] Ishiwara and Jyokyu[26] reported that $SrVO_3$ films directly grown on Si form an insulating interface phase of $SiSrO_3$ because of Si diffusion and depletion of V atoms. Ritums *et al.*[13] used a YSZ buffer layer on an Si substrate to prevent the formation of an insulating $Sr_xSi_yO_z$ interface phase. In Figs. 4(c) and 4(d), $SrVO_3$ films grown on SiO_2/Si (LAO) substrates showed large (small) composition gradients for Sr, V, and O atoms in the layer. Sr content had the most significant composition gradient in $SrVO_3$ films grown on SiO_2/Si substrates, as in Fig. 4(c). Note that $SrVO_3$ films grown on LAO substrates showed sharp interfaces between $SrVO_3$ films and the LAO substrates, similar to $SrVO_3$ films grown on LSAT substrates.

Figure 5 shows (a) the substrate dependence of resistivities for $SrVO_3$ films, (b) the thickness, and (c) the growth temperature dependence of resistivities for $SrVO_3$ films grown on LSAT substrates. For evaluating substrate and growth temperature dependence, the $SrVO_3$ film thickness was fixed at 77 nm. In Fig. 5(b), the resistivity was lowest for $SrVO_3$ films with a thickness of 64 nm grown on LSAT substrates at 400 °C. A growth temperature of 500 °C did not show a noticeable improvement of resistivity values. As shown in Fig. 5(a), various substrates were used to grow low resistivity $SrVO_3$ films; LSAT, SiO_2/Si, c- (a-, m-, r-plane) sapphire, TiO_2 (anatase phase)/Si, and LAO substrates. The smallest resistivity was $0.20 \times 10^{-3}\,\Omega\,cm$ for LSAT. In comparison, the resistivities were $3.29 \times 10^{-3}\,\Omega\,cm$ for SiO_2/Si and $4.03 \times 10^{-3}\,\Omega\,cm$ for LAO substrates. For $SrVO_3$ films with a 77 nm thickness, we measured resistivity as

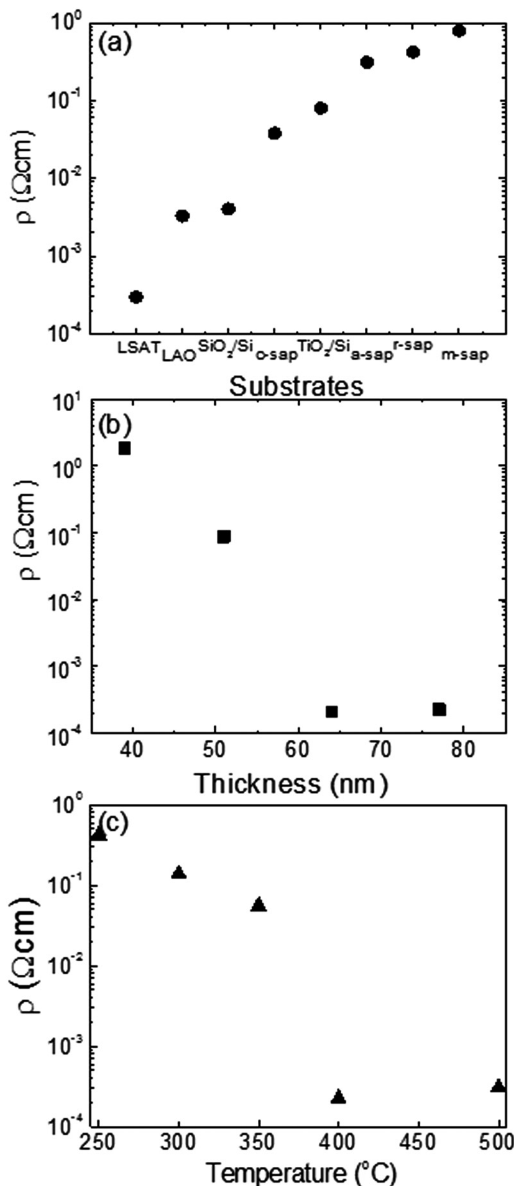

FIG. 5. (a) Substrate dependence of resistivities for $SrVO_3$ films, (b) thickness, and (c) growth temperature dependence of resistivities for $SrVO_3$ films grown on LSAT substrates.

$\rho = 0.22 \times 10^{-3}\ \Omega\,cm$, mobility as $\mu = 1.82\ cm^2/(V\,s)$, and carrier concentration as $N = 1.57 \times 10^{22} cm^{-3}$ using Hall effect measurements. In Table I, we summarized the electrical properties of $SrVO_3$ films and bulk materials grown using various methods in the literature.[4,5,7,14,15] The lowest resistivity values were obtained using hydride MBE, PLD, or laser MBE with LSAT or $SrTiO_3$ substrates.

Figure 6 shows the transmittance of $SrVO_3$ films grown on LSAT substrates with various film thicknesses in the visible spectral range. Transmittance in Fig. 6 reached approximately 88%, 78%, 68%, and 57% at the photon wavelength of 633 nm for $SrVO_3$ films with thicknesses of 39, 51, 64, and 77 nm, respectively. The transmittance of $SrVO_3$/LSAT films was normalized with respect to that of the LSAT substrate. Transmittance was suppressed for energies below 400 nm (i.e., above 3.1 eV), marking the onset of strong interband optical transitions. We note that the transmittance of LSAT substrates is 80%.[4]

We need $SrVO_3$ films with thickness less than 39 nm to achieve a transmittance greater than 90% at 633 nm, because of the rather large extinction coefficient k ($k \approx 0.23$ at $\lambda = 500$ nm) value in the visible range for $SrVO_3$ films.[4] Because of the small mean free path of electron carriers in $SrVO_3$ films, small resistivity values persist even below 10 nm. We note that transmittance is reduced by decreasing the film thickness in several p-type TCOs such as SnO, TaIrGe, and boron phosphide, because they have weak absorption in the visible range.[32]

Raman spectra showed no peaks from $SrVO_3$ films and showed only peaks from LSAT substrates (not shown here). This phenomenon is consistent with Raman selection rules which require no Raman-active peaks in $SrVO_3$ films.[33]

The satellite peaks for $SrVO_3$ films, shown in Fig. 3(c), may arise from Jahn-Teller distortion in $SrVO_3$ films. Oxygen defects may cause change of valences of vanadium atoms which can induce crystal fields and generate Jahn-Teller distortion.[34] The Jahn-Teller distortion may have induced distortion of cubic unit cells in $SrVO_3$ and produced spontaneous formation of superstructures which have periodicities of four to five unit cells. In general, Jahn-Teller distortions occur in e_g systems such as perovskite manganites (e.g., $La_{1/3}Ca_{2/3}MnO_3$).[35,36] However, weak Jahn-Teller distortion are found in perovskite vanadates such as YVO_3, $LaVO_3$, and $SrVO_3$ even though they are t_{2g} systems.[37–39] According to HRTEM data [Fig. 3(c)], cubic $SrVO_3$ may have been transformed into an orthorhombic system possibly due to Jahn-Teller distortion or ordering of oxygen vacancies. More detailed HRTEM study are currently in progress to understand more accurately the origin of satellite structures. Jahn-Teller distortion is accompanied with distortion of MO_6 bonds along bond direction (i.e., along M–O direction) in e_g systems. In t_{2g} system, Jahn-Teller distortion is associated with the distortion in planar MO_4 squares, where the distortion occurs off the M–O bond direction.[39] Jahn-Teller distortion in ultrathin $SrVO_3$ films were proposed using density functional theory by Gupta *et al.*[34]

XPS analysis of vanadium ion valence states for $SrVO_3$ films in Fig. 5(a) shows that the increase of the valence state ratio of V^{4+}/V^5+ is correlated with the decrease of resistivities with increasing $SrVO_3$ film thickness, as in Fig. 5(b). This phenomenon may be attributed to the amorphous $Sr_2V_2O_7$ phase (or orthorhombic $SrVO_3$ phase) that is dominant at the surface of thin "$SrVO_3$" films, the proportion of crystalline $SrVO_3$ phase increases with increasing thickness, and the $SrVO_3$ phase is dominant for 77-nm-thick $SrVO_3$ films. This explains why the thicker $SrVO_3$ films show a lower resistivity than thinner films (Fig. 6).

The XPS depth profile analysis in Figs. 5(b) and 5(c) shows that the depth profile of $SrVO_3$ compositions is constant for LSAT substrates whereas those of LAO and SiO_2/Si substrates are depth-dependent. The composition gradients of Sr, V, and O atoms were negligible for $SrVO_3$/LSAT, were largest for $SrVO_3/SiO_2$/Si, and were moderate for $SrVO_3$/LAO. A large composition gradient means inhomogeneity of

TABLE I. Electrical properties of the bulk and thin film $SrVO_3$ at 300 K in the literature.

ρ ($\times10^{-3}$ Ω cm)	N ($\times10^{22}$ cm^{-3})	μ [cm^2/(V s)]	Substrate	Growth method	Reference
0.22	1.57	1.82	LSAT	Sputtering deposition	This work (thickness 77 nm)
0.03	2.26	9.0	LSAT	Hydride MBE	4
0.12	2.18	3.05	LSAT	PLD	6
0.045	3.25	0.81	$SrTiO_3$	PLD	15
0.117	3.0	1.9	LSAT	Pulsed electron-beam deposition	9
0.11			$LaAlO_3$	PLD	13
0.28			$SrTiO_3$	PLD	27
0.34			Si	E-beam evaporation	8
0.05			$SrTiO_3$	Laser MBE	14
2.5				Solid reaction (bulk)	28
0.222				Solid reaction (bulk)	29
41.8				Solid reaction (bulk)	30
0.75				Solid reaction (bulk)	31

$SrVO_3$ films and excess or deficiency of Sr, V, and O atoms compared to the stoichiometric $SrVO_3$ films.[18] In the case of LSAT substrates, $SrVO_3$ films and LSAT substrates were almost lattice-matched and high-quality $SrVO_3$ films grew without severe misfit strain. Therefore, $SrVO_3$/LSAT showed the smallest resistivity among $SrVO_3$/LAO and $SrVO_3$/SiO_2/Si [Fig. 5(a)]. Note that $SrVO_3$/SiO_2/Si produced an insulating Sr_xV_yO phase rather than a $SrVO_3$ phase in the interface; thus, the resistivity increased with the increase of Sr_xV_yO phase content.

In Fig. 4(a), the binding energy of V decreased from 516.83 eV (39 nm, V^{5+}) to 516.30 eV (77 nm, V^{4+}) as the film thickness increased. XPS is a surface-sensitive probe because it measures the kinetic energy of emitted electrons by incident x-ray. About 10 nm from the surface can be probed using XPS. It seems that surface oxide ($Sr_2V_2O_7$) layer thickness decreased with increasing $SrVO_3$ film thickness. Then, the volume ratio of the surface oxide layer to the main layer will decrease with increasing film thickness.

We measured resistivity as $\rho = 0.22 \times 10^{-3}$ Ω cm, mobility as $\mu = 1.82$ cm^2/(V s), and carrier concentration as $N = 1.57 \times 10^{22}$ cm^{-3} using Hall effect measurements for $SrVO_3$ films with 77 nm thickness grown using RF sputtering deposition methods. The resistivity value is comparable to those of PLD-grown $SrVO_3$ films of Boileau *et al.*,[6] whereas the resistivity value is an order of magnitude larger than the resistivity of 0.03×10^{-3} Ω cm obtained for $SrVO_3$ films grown using hybrid MBE.[4,5] Boileau *et al.*[6] maintained that high-quality $SrVO_3$ films can be grown with temperatures as low as 400 °C using PLD, and that a front-end-of-line application such as TCO may be possible. Sputtering deposition method is a general-purpose deposition method and is widely used in industries because of its simplicity. This work shows that sputtering deposition of $SrVO_3$ films grown at 400 °C can be comparable to more sophisticated PLD-grown films, which expands the potential applications of $SrVO_3$ films as TCO materials.

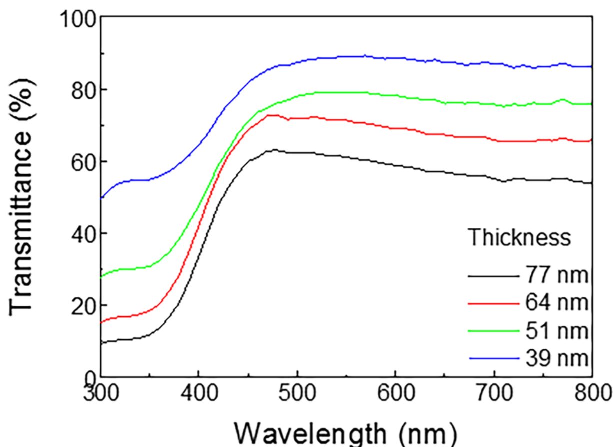

FIG. 6. Transmittance spectra of $SrVO_3$ films grown on LSAT substrates with various film thicknesses in the visible spectral range.

IV. CONCLUSION

We grew transparent conductor $SrVO_3$ films on various substrates with commercial $Sr_2V_2O_7$ targets using RF magnetron sputtering deposition. We used a 25% H_2 and Ar mixed gas atmosphere during growth to obtain $SrVO_3$ films from $Sr_2V_2O_7$ targets via reduction. The lowest resistivity value of 0.20×10^{-3} Ω cm was obtained using almost lattice-matched LSAT substrates at a growth temperature of 400 °C with $SrVO_3$ film thickness of 64 nm. Resistivity values of 3.29×10^{-3} and 4.03×10^{-3} Ω cm were obtained for SiO_2/Si and $LaAlO_3$ substrates, respectively. Superstructures comprised of four or five unit cells were found using HRTEM and were attributed to Jahn-Teller distortion. Using x-ray photoemission spectroscopy and its depth profile analysis, we found correlation among the resistivities, V^{4+}/V^{5+} valence state ratio, and composition gradients of Sr, V, and O atoms. This work demonstrates that high-quality $SrVO_3$ films can be grown on LSAT substrates at temperatures as low as 400 °C as TCO films for use in high throughput and low cost indiumfree transparent electrodes.

ACKNOWLEDGMENTS

H.L. was supported by the National Research Foundation of Korea (No. NRF-2016R1D1A1B03930725). H.L. thanks Jong Soo Rhyee at Kyung Hee University and Woo Seok Choi at Sungkyunkwan University for discussion on Jahn-Teller distortion.

[1]Q. Zhou, Z. Ji, B. B. Hu, C. Chen, L. Zhao, and C. Wang, Mater. Lett. **61**, 531 (2007).
[2]T. Minami, MRS Bull. **25**, 38 (2000).
[3]X. Zhang, L. Zhang, J. D. Perkins, and A. Zunger, Phys. Rev. Lett. **115**, 176602 (2015).
[4]L. Zhang *et al.*, Nat. Mater. **15**, 204 (2016).
[5]J. A. Moyer, C. Eaton, and R. Engel-Herbert, Adv. Mater. **25**, 3578 (2013).
[6]A. Boileau, A. Cheikh, A. Fouchet, A. David, R. Escobar-Galindo, C. Labbé, P. Marie, F. Gourbilleau, and U. Lüders, Appl. Phys. Lett. **112**, 021905 (2018).
[7]B. Bérini, V. Demange, M. Bouttemy, E. Popova, N. Keller, Y. Dumont, and A. Fouchet, Adv. Mater. Interface **3**, 1600274 (2016).
[8]B. K. Moon and H. Ishiwara, J. Cryst. Growth **162**, 154 (1996).
[9]M. Gu, S. A. Wolf, and J. Lu, Adv. Mater. Interface **1**, 1300126 (2014).
[10]D. L. Ritums, N. J. Wu, D. Liu, Q. Zhong, Y. M. Chen, X. Zhang, P. C. Chou and A. Ignatiev, *ISAF '96. Proceedings of the Tenth IEEE International Symposium on Applied Ferroelectrics* East Brunswick, NJ, 18–23 August 1996 (IEEE, Piscataway, NJ 1996), pp. 417–420.
[11]D. W. Jung, H. J. Park, C. Kwak, B. Ryu, and K. H. Lee, U.S. patent no. US 9,659,681 B2 (23 May 2017).
[12]A. Sharma, M. Varshney, W. C. Lim, H.-J. Shin, J. P. Singh, S. O. Won, and K. H. Chae, Phys. Chem. Chem. Phys. **19**, 6397 (2017).
[13]D. L. Ritums, N. J. Wu, X. Chen, D. Liu, and A. Ignatiev, AIP Conf. Proc. **420**, 672 (1998).
[14]H. Nagata, T. Tsukahara, M. Yoshimoto, and H. Koinuma, Thin Solid Films **208**, 264 (1992).
[15]A. Fouchet *et al.*, Mater. Sci. Eng. B **212**, 7 (2016).
[16]H. Nagata, Thin Solid Films **224**, 1 (1993).
[17]M. Brahlek, L. Zhang, C. Eaton, H.-T. Zhang, and R. Engel-Herbert, Appl. Phys. Lett. **107**, 143108 (2015).
[18]Joint Committee on Powder Diffraction Standards, International Center for Diffraction Data, No. 81-0119.
[19]M. J. Rey, Ph. Dehaudt, J. C. Joubert, B. Lambert-Andron, and M. Cyrot, J. Solid State Chem. **86**, 101 (1990).
[20]Joint Committee on Powder Diffraction Standards, International Center for Diffraction Data, No. 32-1267.
[21]Joint Committee on Powder Diffraction Standards, International Center for Diffraction Data, No.71-1593.
[22]C. Eaton, J. A. Moyer, H. M. Alipour, E. D. Grimley, M. Brahlek, J. M. LeBeau, and R. Engel-Herbert, J. Vac. Sci. Technol. A **33**, 061504 (2015).
[23]T. N. Nunley, T. I. Willett-Gies, J. A. Cooke, F. S. Manciu, P. Marsik, C. Bernhard, and S. Zollner, J. Vac. Sci. Technol. A **34**, 051507 (2016).
[24]G. Silversmit, D. Depla, H. Poelman, G. B. Marin, and R. De Gryse, J. Electron Spectrosc. Relat. Phenom. **135**, 167 (2004).
[25]T. Miruszewski, B. Kamecki, M. Łapiński, and J. Karczewski, Mater. Chem. Phys. **212**, 446 (2018).
[26]H. Ishiwara and K. Jyokyu, Jpn. J. Appl. Phys. **30**, L2059 (1991).
[27]Q.-R. Li, M. Major, M. B. Yazdi, W. Donner, V. H. Dao, B. Mercey, and U. Lüders, Phys. Rev. B **91**, 035420 (2015).
[28]V. Giannakopoulou, P. Odier, J. M. Bassat, and J. P. Loup, Solid State Commun. **93**, 579 (1995).
[29]P. Dougier, J. C. C. Fan, and T. J. B. Goodenough, J. Solid State Chem. **14**, 247 (1975).
[30]Y. C. Lan, X. L. Chen, and M. He, J. Alloys Compd. **354**, 95 (2003).
[31]T. Maekawa, K. Kurosaki, and S. Yamanaka, J. Alloys Compd. **426**, 46 (2006).
[32]L. Hu *et al.*, Adv. Electon. Mater. **4**, 1700476 (2018).
[33]H. Makino, I. H. Inoue, M. J. Rozenberg, I. Hase, Y. Aiura, and S. Onari, Phys. Rev. B **58**, 4384 (1998).
[34]K. Gupta, P. Mahadevan, P. Mavropoulos, and M. Ležaić, Phys. Rev. Lett. **111**, 077601 (2013).
[35]P. G. Radaelli, D. E. Cox, L. Capogna, S.-W. Cheong, and M. Marezio, Phys. Rev. B **59**, 14440 (1999).
[36]A. J. Millis, Nature **392**, 147 (1998).
[37]T. Mizokawa, D. I. Khomskii, and G. A. Sawatzky, Phys. Rev. B **60**, 7309 (1999).
[38]H. Meley, Karandeep, L. Oberson, J. de Bruijckere, D. T. L. Alexander, J.-M. Triscone, Ph. Ghosez, and S. Gariglio, APL Mater. **6**, 046102 (2018).
[39]S. Maekawa, T. Tohyama, S. E. Barnes, S. Ishihara, W. Koshibae, and G. Khaliullin, *Physics of Transition Metal Oxides* (Springer-Verlag, Berlin, 2004).

View publication stats